Asian Journal of Chemistry; Vol. 32, No. 3 (2020), 555-560

ASIAN JOURNAL OF CHEMISTRY

https://doi.org/10.14233/ajchem.2020.21991

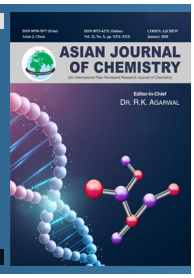

Physico-Chemical Properties of Nickel Promoted Sulfated Zirconia Powder Prepared using Different Procedures

AMALIA KURNIA AMIN, KARNA WIJAYA* and WEGA TRISUNARYANTI

Department of Chemistry, Faculty of Mathematics and Natural Sciences, Universitas Gadjah Mada, Sekip Utara Bulaksumur, Yogyakarta 55281, Indonesia

*Corresponding author: E-mail : karnawijaya@ugm.ac.id

Received: 8 February 2019; *Accepted*: 20 October 2019; *Published online*: 31 January 2020; AJC-19757

In this work, nickel promoted sulfated zirconia (Ni/SZ) as catalyst was prepared by either by reflux (Ni/SZ-R) or hydrothermal Ni impregnation (Ni/SZ-H) routes. The aim of this study was to evaluate the influences of two preparative methods on the physico-chemical properties of prepared catalysts. Both the catalysts were characterized by XRD, FTIR, ammonia adsorption, SEM-EDX, TEM-SAED, AAS and BET. It was found that the presence of sulfate and nickel could enhance the Brønsted and Lewis active acid sites. In relation to the effect of Ni impregnation method, acidity, amount of sulfate and Ni found in Ni/SZ-R were higher than those in Ni/SZ-H. Unfortunately, higher impregnated sulfate and nickel on zirconia support led to a decrease in surface area and pore volume and an increase in crystallite size of grainy aggregated mesoporous nickel promoted sulfated zirconia (Ni/SZ).

Keywords: Nickel, Sulfated zirconia, Reflux method, Hydrothermal method.

INTRODUCTION

Bifunctional catalysts are still a promising industrial-scale catalysts, thus are widely studied [1]. Bifunctional catalysts are characterized by the presence of both acid and metal sites. Acid sites usually come from porous solid support like alumino-silicate, alumina, zirconia and sulfated zirconia, while the metal sites are facilitated by supported metal, such as Pt, Pd, Fe, Ni, Mo and Mn [2-7]. These catalysts are widely applied in hydro-reforming reactions, such as hydrocracking, hydroisomerization, hydrodesulfurization, hydrodenitrification and visbreaking [2-7]. Catalysts based on metal-promoted sulfated zirconia have attracted much attention due to their thermal stability, strong acidity, coke tenacity and reusability as a bifunctional solid acid catalyst [7-9]. The catalytic performance of metal-promoted sulfated zirconia mainly depends on its supported metal content and acidity which act as its active surface sites [8,10]. In addition, morphology, crystal phase, specific surface area and porosity of metal-promoted sulfated zirconia also affect its reactivity [8,11]. Those physico-chemical properties were strongly influenced by the natural properties of precursors, methods of preparation and reaction conditions of preparation [8,10,12].

Noble metals such as platinum and palladium are known to have a high reactivity toward hydrogenation-dehydrogenation and organic compound transformation. Compared to noble metals, nickel is one of the most promising non-noble metals to facilitate hydrogenation/dehydrogenation functions and versatile catalytic ability [3] to prevent the use of other expensive catalysts for economic and technological reasons. Moreover, nickel is abundant and environmentally benign. The most common nickel impregnation method used is incipient wetness impregnation [7,13]. In this paper, as different methods, both reflux and hydrothermal impregnation of nickel over sulfated zirconia were carried out. The catalysts prepared by both methods were performed in order to evaluate which method provides the proper combination of physico-chemical properties of nickel promoted sulfated zirconia (Ni/SZ).

EXPERIMENTAL

Zirconia with a purity of 99.9 % and 60-70 nm in size was purchased from Jiaozou Huasu Chemical Co. Ltd. The sulfuric acid, nickel nitrate hexahydrate and ammonium hydroxide were purchased from Merck and used as received. Meanwhile, hydrogen gas was supplied by PT. Samator Gas Co., Indonesia.

Catalysts preparation: Sulfated zirconia was prepared by calcining slurry material obtained from wet impregnation of sulfuric acid (0.8 M) on commercial zirconia (ZrO_2) at 400 ºC for 4 h as per literature method [8]. A sample of nickel promoted sulfated zirconia was initially prepared by refluxing sulfated zirconia powder with 50 mL aqueous solution of nickel nitrate hexahydrate that corresponded to 1.5 wt.% of Ni at 90 ºC for 4 h under magnetic stirrer system. Subsequently, slurry material sample was dried overnight at 120 °C, followed by calcination in the air at 500 °C for 4 h and reduction under hydrogen gas stream (20 mL/min) at 400 °C for 3 h.

Using hydrothermally process, nickel promoted sulfated zirconia catalyst was initially prepared by adding sulfated zirconia powder in 50 mL aqueous solution of nickel nitrate hexahydrate (1.5 wt.% of Ni) in Teflon vessel contained in a stainless steel autoclave without magnetic stirrer system at 90 ºC for 4 h. Subsequently, slurry material sample was dried overnight at 120 ºC, followed by calcination in the air at 500 ºC for 4 h and reduction under hydrogen gas stream (20 mL/min) at 400 ºC for 3 h.

Characterization: Fourier transform infrared (FTIR) spectra were recorded on Shimadzu Prestige-21 using KBr for identifying functional groups and evaluating further acidic types based on the adsorbed ammonia species on the catalysts. A catalyst acidity value was measured by using the gravimetric method. The acidity value [mmol NH_3/g catalyst] is equal to the different weights of catalyst after and before ammonia adsorption and was divided by multiplication of catalyst weight before ammonia adsorption with the molecular weight of ammonia [17.007 g/mol].

X-ray diffractometer (XRD, Rikagu Multiflex) equipped with Cu *K*α lamp and Ni filter was used for crystal structure identification and crystallite size determination. Diffraction patterns were scanned in the 2θ range from 10º to 60º. Crystallite size (D in nm) was determined using Scherrer formula $D = k\lambda/B\cos\theta$, where k is a shape factor [0.89], λ is the wavelength of Cu *K*α [0.15418 nm], B is the full width at half maximum of peak in radian and θ is Bragg angle. The Brunauer-Emmett-Teller (BET) surface area and porosity were determined by recording nitrogen adsorption-desorption isotherms at 77.3 K using a static volumetric technique with a gas sorption analyzer (GSA, Quantachrome NOVA 11.0). The surface topography was characterized by a field emission scanning electron microscope with energy dispersive X-ray spectroscopy (SEM-EDX, JEOL JSM-6510 JED-2300). The morphology was estimated by a transmission electron microscope (TEM, JEOL JEM-1400) with a selected area electron diffraction (SAED). The amount of nickel contained was determined by an atomic absorption spectroscopy (AAS, ContrAA 300 Analytic Jena). Previously, the samples were digested by acid treatment with HF and aqua regia.

RESULTS AND DISCUSSION

FTIR analyses and acidic properties: The formation of sulfated zirconia occurred through the interaction of sulfate ions with Zr atoms from ZrO_2 which tended to have a positive partial charge, continuing with the formation of covalent coordination bonds between them. Therefore, spectrometric analysis using FTIR could be used to prove the success of sulfated zirconia catalyst preparation. Unfortunately, interaction of Ni metal with sulfated zirconia in Ni/SZ catalyst system could not be detected due to the non-formation of covalent bond. Fig.1a shows the FTIR spectra of ZrO_2, sulfated zirconia (SZ), and Ni/SZ-R catalysts. Based on Fig. 1a, in addition to the emergence of absorption bands at around 750-500, 1630 and 3400 cm^{-1}, which are typical of Zr-O-Zr stretching, H-O-H bending and O-H stretching frequencies, respectively. Both SZ and Ni/SZ-R gave absorption bands at 1250-1000 cm^{-1} which are typical of the symmetric and asymmetric vibration band of S-O stretching and S=O stretching from bidentate chelation of sulfate ions [8,10,14]. The appearance of those additional bands indicated the presence of an impregnated sulfate group in ZrO_2 as a support material. A decrease in the

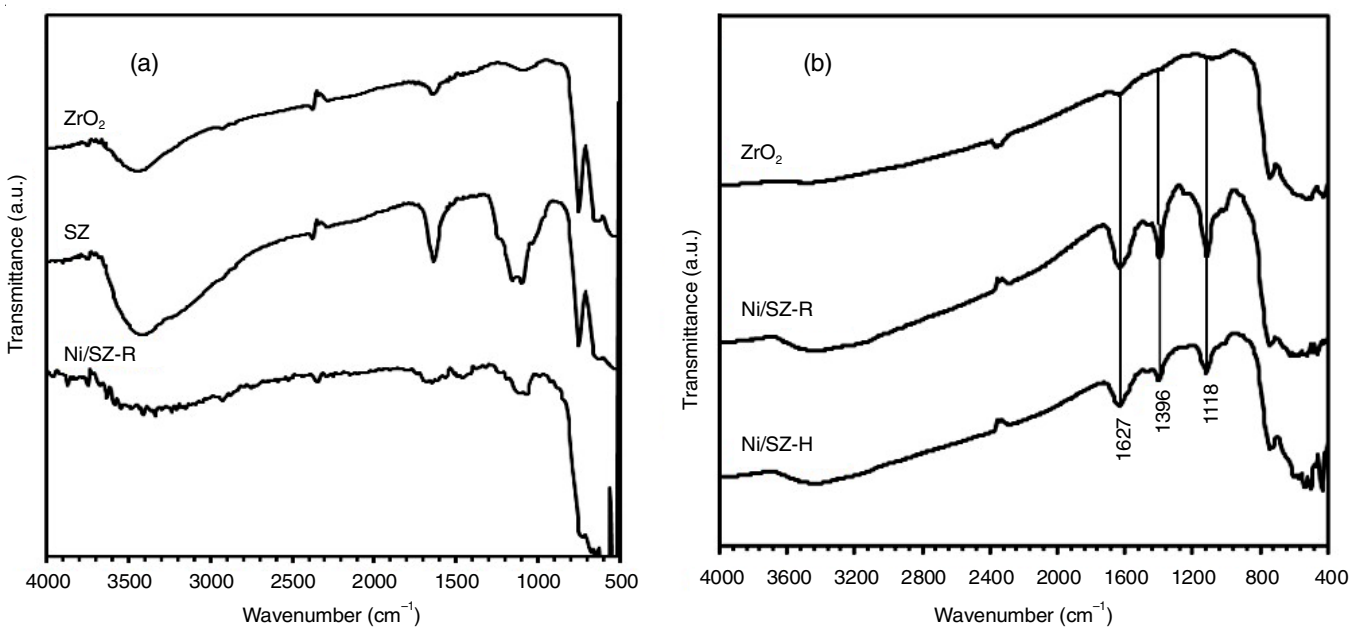

Fig. 1. FTIR spectra of (a) catalysts and (b) ammonia sorbed on the catalysts

intensity of sulfate group absorption band from Ni/SZ-R catalyst when compared to sulfated zirconia catalyst reflected decreasing sulfate dispersion that was believed to be associated with the release of some sulfate groups as a result of the reflux or hydrothermal treatments involving water and recurrent heat treatment, including re-calcination and reduction of nickel.

Sulfate and nickel were responsible for the sites of Brønsted and Lewis acids, acted as active sites of Ni/SZ which had important effects on the catalytic activity [8,15]. The strength or amount of acid sites in Ni/SZ-R and Ni/SZ-H catalysts could be qualitatively identified using FTIR spectroscopy based on the adsorbed ammonia probes [8,11,16]. The absorption bands centered around 1118 and 1627 cm^{-1} were related to the vibrations of ammonia coordinated to Lewis acid sites, while the absorption band at 1396 cm^{-1} was attributed to ammonium ion coordinately bonded to Brønsted acid in the catalyst material [16-18]. Fig. 1b shows the difference of FTIR spectra obtained after the adsorption of ammonia. The acidity of Ni/SZ catalysts were increased by the incorporation of sulfate and nickel. However, acid sites found in Ni/SZ-R were more than that of Ni/SZ-H. The appearance of FTIR band at around 1600-1000 cm^{-1} region was strongly dependent on the Ni impregnation preparative method. Compared to Ni/SZ-H, which was prepared using the hydrothermal method, Ni/SZ-R that was prepared the reflux method gave stronger intensity of both Lewis acid and Brønsted acid vibrational bands. The gravimetric measurement of ZrO_2, Ni/SZ-R and Ni/SZ-H catalysts revealed that their respective total acidities were 0.11, 2.70 and 2.61 mmol ammonia/g catalyst. The preparation performed in the presence of magnetic stirring on the reflux method was much more effective to impregnated of Ni without losing to much sulfate group since the total acidity of Ni/SZ-R was higher than Ni/SZ-H.

XRD analysis: Fig. 2 shows the XRD patterns of ZrO_2 and Ni/SZ catalysts prepared by different preparative methods with the same amount of Ni precursor. The crystalline phase of those modified and unmodified ZrO_2 seemed similar. The XRD phase analysis revealed that all catalysts consisted a monoclinic ZrO_2, gave diffraction peak at 2θ of about 28.2º and 31.5º, assigned to $\bar{1}11$ and 111 of monoclinic crystal phase

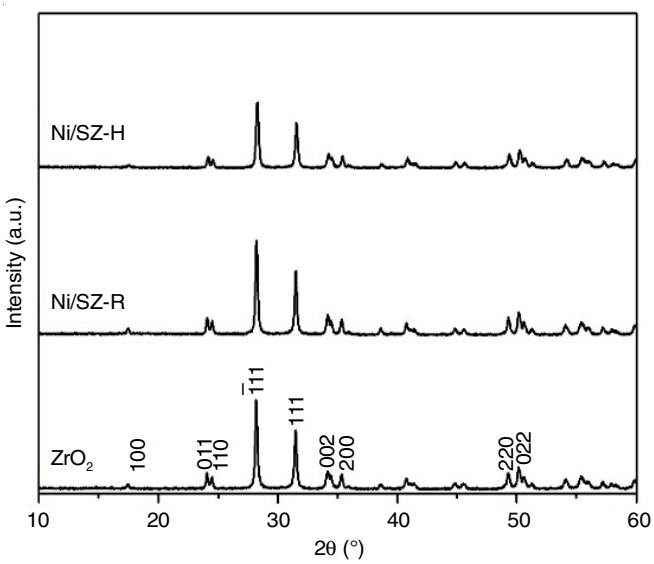

Fig. 2. XRD patterns of catalysts

of ZrO_2 [19]. Basically, it is known that beside amorphous ZrO_2, ZrO_2 crystalline has three polymorphs, namely monoclinic, tetragonal and cubic. The stable polymorph of ZrO_2 at room temperature up to 1140 ºC is the monoclinic phase [1]. The metastable tetragonal phase is known to be stabilized by the formation of nano-grained ZrO_2 and by impregnating of metal into ZrO_2 [10], but in present research, metastable tetragonal ZrO_2 did not form. This phenomena happened because of the Ni promotor was too low so it could not generate the phase transformation of ZrO_2. Moreover, there was no diffraction peak of crystalline phase of Ni metal (Ni^0) observed in the diffraction patterns of Ni/SZ-R and Ni/SZ-H, indicating the low valency of Ni on the catalyst and highly dispersed of Ni species on the sulfated zirconia (SZ) support [7]. The crystallite sizes of ZrO_2, Ni/SZ-R and Ni/SZ-H were 44.50, 44.98 and 44.51 nm, respectively. The crystallite size increased as the incorporation of sulfate and nickel.

Electron microscopy analyses and elemental analyses: The SEM images of Ni/SZ-R and Ni/SZ-H are shown in Fig. 3. The images revealed that both catalysts were composed of grainy irregular aggregated particles. The aggregate particles of Ni/SZ-H had relatively the same size as compared to those of Ni/SZ-R. The particles of Ni/SZ-R were in a lump shape, while those of Ni/SZ-H were in a flake shape. More disordered shapes were also obtained in Ni/SZ-R.

The elementals on the surface of Ni/SZ-R and Ni/SZ-H were analyzed by EDX as shown in Fig. 3 and Table-1. Total Ni in Ni/SZ-R and Ni/SZ-H was determined by AAS and listed in Table-1. The sulfated zirconia (SZ) support and Ni precursor used for preparation of Ni/SZ-R and Ni/SZ-H were in the same ratio, but the observed values of Zr, O, S and Ni on the surface of Ni/SZ-R were higher. It indicated the leaching or loss of sulfate group from the surface of sulfated zirconia during nickel impregnation in the reflux processing was lower than that in the hydrothermal processing. The retention of sulfate was better under the reflux processing. As a function of different of preparative methods, Ni dispersion on the surface of Ni/SZ-R was also better. The facts showing that two catalysts having almost same total Ni but the amounts of Ni on their surface were dramatically different, suggested that most of Ni in Ni/SZ-H was entering and filling the pores or the internal surface of the materials, so it did not exposure on the external surfaces.

TABLE-1
ELEMENTAL CONTENTS OF CATALYSTS

Sample	Element composition (wt. %)				
	Zr[a]	O[a]	S[a]	Ni[a]	Ni[b]
Ni/SZ-R	68.09	30.01	0.56	1.34	1.15
Ni/SZ-H	71.81	27.81	0.41	0.43	1.14

[a]Element on the surface (SEM-EDX); [b]Total element (AAS)

The TEM images of Ni/SZ-R was almost same as compared to Ni/SZ-H (Fig. 4). Both the catalysts exhibited aggregate particles. The particles seem semispherical in shape. There were Ni aggregates on the external surface of sulfated zirconia aggregates, marked by the appearance of small lighter spots surrounding the large dark spots [8]. The SAED analysis confirmed that the catalysts were composed of crystallized materials as the SAED diffraction patterns gave bright dotted spots

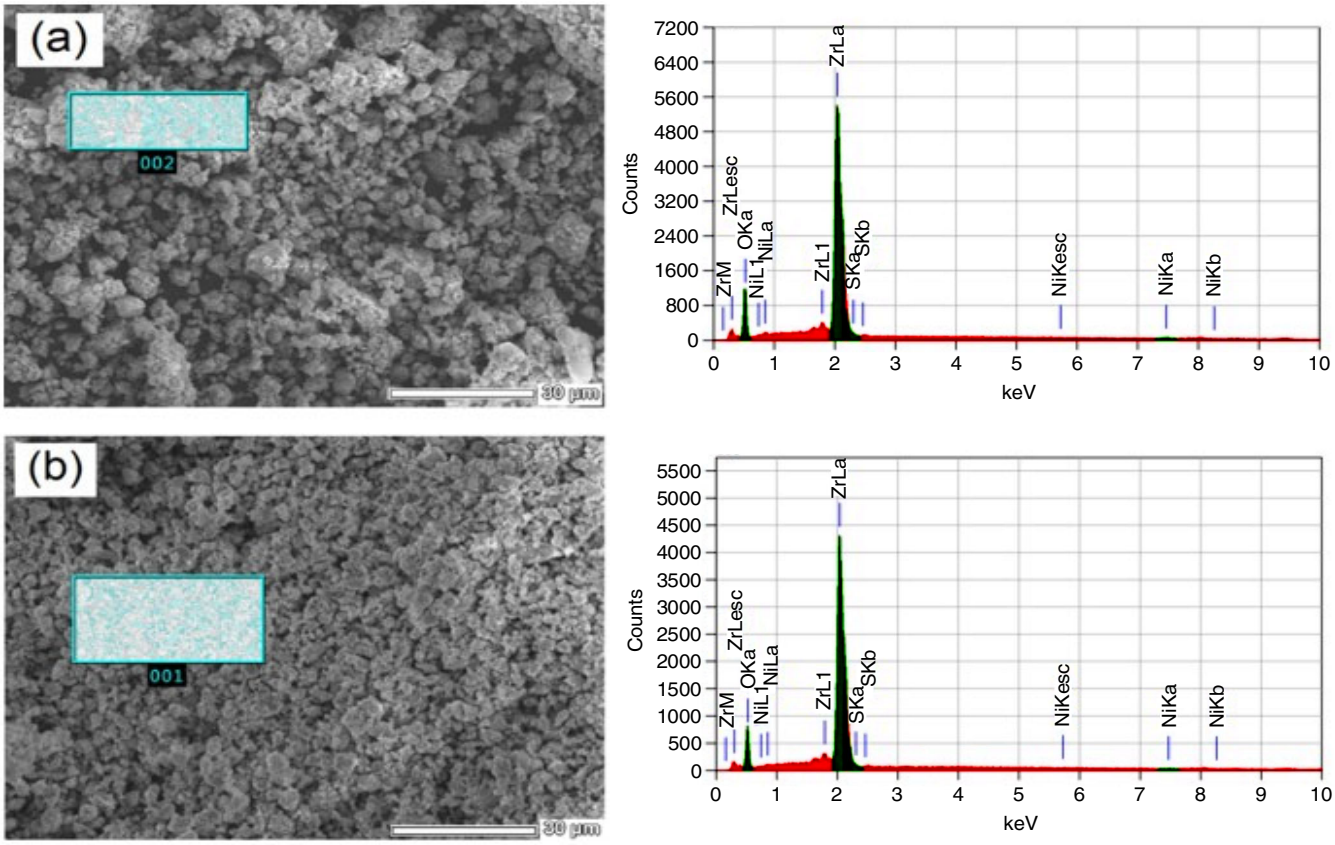

Fig. 3. SEM micrograph and EDX spectra of (a) Ni/SZ-R and (b) Ni/SZ-H catalysts

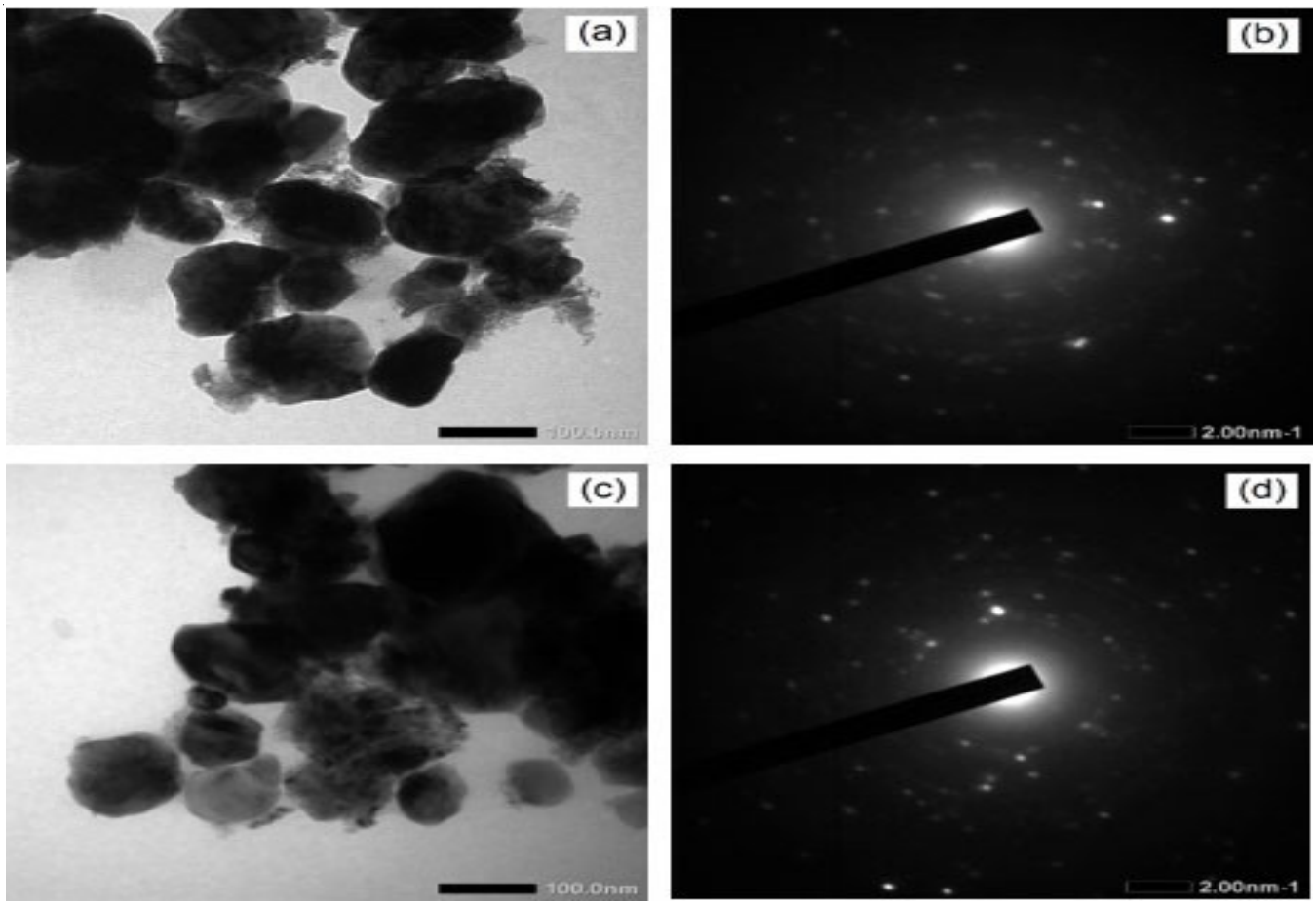

Fig. 4. TEM micrograph and SAED pattern of (a,b) Ni/SZ-R and (c,d) Ni/SZ-H catalysts

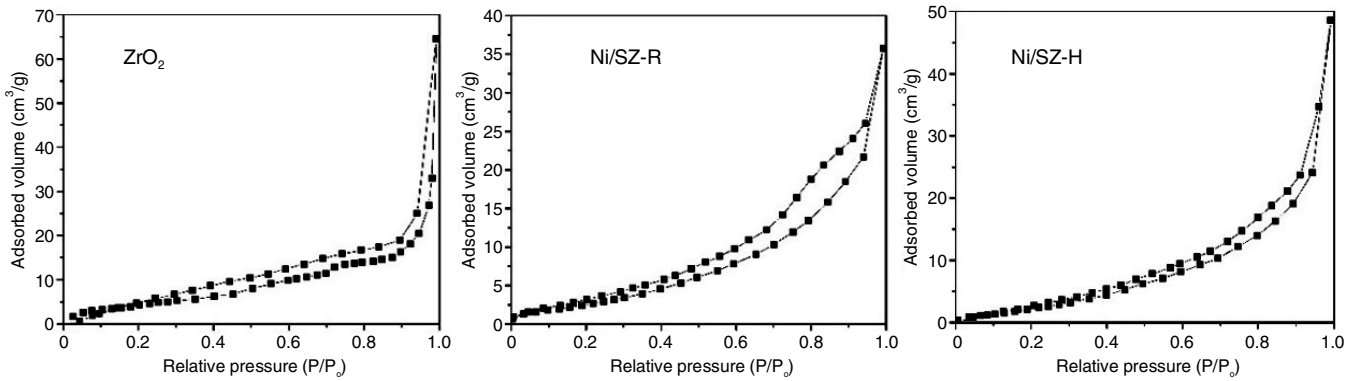

Fig. 5. N_2 adsorption-desorption isotherms of catalysts

patterns which corresponded to a single-crystal diffraction. As shown in Fig. 4, a combination of spots also made up rings corresponding to powder diffraction of polycrystalline [20].

Brunauer-Emmett-Teller (BET) surface area analysis: Nitrogen gas adsorption was a well-established way for determining the surface area and the porosity of fine powder and porous materials. The adsorption-desorption isotherm is shown in Fig. 5. According to the 1985 IUPAC physisorption isotherms classification, all catalysts are characterized as mesoporous material since they displayed type IV isotherm. The adsorption behaviour in mesopores is determined by the adsorbent-adsorptive interactions and also by the interactions between the molecules in the condensed state. Basically, emergence of hysteresis loop comes from pore condensation phenomenon (capillary condensation) [21,22]. Hysteresis starts to occur for pores wider than ~ 4 nm [22]. All catalysts have type H3 hysteresis loop. This type are given by non-rigid aggregate of plate-like particles that create slit-shaped pores or if the pore network consists of macropores which were not completely filled with pore condensates [21,22]. The pore size distribution of Ni/SZ-R and Ni/SZ-H were estimated by the BJH method. As shown in Fig. 6, the catalysts consisted of some macropores (50-76 nm) [2]. The Ni/SZ-R gave wider pore size distribution than Ni/SZ-H. The average pore diameters of those catalysts are listed in Table-2.

The surface areas, average pore diameters and total pore volumes values are summarized in Table-2. As expected from

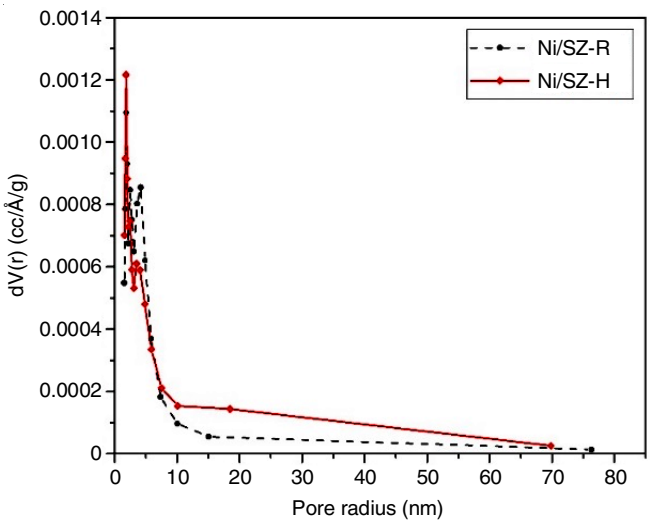

Fig. 6. Pore size distribution of catalysts

TABLE-2
TEXTURAL OF CATALYST

Sample	S_{BET} (m^2/g)	V_P (cm^3/g)	Pore diameter (nm)
ZrO_2	17.37	0.099	23.00
Ni/SZ-R	10.57	0.055	20.92
Ni/SZ-H	14.30	0.075	20.60

the isotherms, both Ni/SZ-R and Ni/SZ-H gave lower BET surface areas than ZrO_2. This was due to that sulfate and Ni dispersed on the surface of ZrO_2 partly filled or even blocked the pores and finally affected on the pore volume to drop. However, surface area and total pore volume of Ni/SZ-H was larger than those of Ni/SZ-R, although the average pore diameter of Ni/SZ-H was smaller. Since, the average pore diameter was smaller in the larger surface area and total pore volume, it was suggested that that nickel was highly dispersed on the internal surface and filled in the pores of porous Ni/SZ. This was associated with the amount and the location of impregnated sulfate and Ni on ZrO_2 support materials [8,23]. The results are in accordance with the data resulted from the elemental analyses.

Conclusion

The impregnation of nickel promotor *via* refluxing and hydrothermal methods successfully resulted mesoporous of polycrystalline Ni/SZ materials which had higher acid strength than commercial ZrO_2 but consequently had lower surface area. Total Ni present in Ni/SZ-R and Ni/SZ-H were almost the same, namely 1.15 *versus* 1.14 wt.%, respectively. The surface topography and mesoporosity of Ni/SZ-R and Ni/SZ-H were slightly different. The observation found grainy lump-shaped aggregated particles of Ni/SZ-R with higher sulfate and Ni on the surface and wider pore diameter. Meanwhile, Ni/SZ-H was found as grainy flake-shaped aggregated particles, which had a lower amount of sulfate and Ni on the external surface area.

ACKNOWLEDGEMENTS

The authors are grateful for financial support from Indonesian Ministry of Research, Technology and Higher Education (DRPM-DIKTI) through PMDSU Batch II Research Grant (Project trace PMSDU 2027/UN1/DITLIT/DIT-LIT/LT/2018).

CONFLICT OF INTEREST

The authors declare that there is no conflict of interests regarding the publication of this article.

REFERENCES

1. G.D. Yadav and J.J. Nair, *Micropor. Mesopor. Mater.*, **33**, 1 (1999); https://doi.org/10.1016/S1387-1811(99)00147-X
2. K. Wijaya, *Indones. J. Chem.*, **2**, 142 (2002); https://doi.org/10.22146/ijc.21909
3. J.M. Escola, J. Aguado, D.P. Serano, L. Briones, J.L. Díaz de Tuesta, R. Calvo and E. Fernandez, *Energy Fuels*, **26**, 3187 (2012); https://doi.org/10.1021/ef300938r
4. N. Insura, J.A. Onwudili and P.T. Williams, *Energy Fuels*, **24**, 4231 (2010); https://doi.org/10.1021/ef100227f
5. W. Ding, J. Liang and L.L. Anderson, *Energy Fuels*, **11**, 1219 (1997); https://doi.org/10.1021/ef970051q
6. S.X. Song, M. Pilko and R.A. Kydd, *Catal. Lett.*, **55**, 97 (1998); https://doi.org/10.1023/A:1019022610103
7. P. Jing, Q. Li, M. Han, D. Sun, L. Jia and W. Wang, *Front. Chem. Eng. China*, **2**, 186 (2008); https://doi.org/10.1007/s11705-008-0035-y
8. A.K. Amin, K. Wijaya and W. Trisunaryanti, *Orient. J. Chem.*, **34**, 3070 (2018); https://doi.org/10.13005/ojc/340650
9. Y. Song, J. Tian, Y. Ye, Y, Jin, X. Zhou, J. Wang and L. Xu, *Catal. Today*, **212**, 108 (2013); https://doi.org/10.1016/j.cattod.2012.07.024
10. M. Utami, K. Wijaya and W. Trisunaryanti, *Mater. Chem. Phys.*, **213**, 548 (2018); https://doi.org/10.1016/j.matchemphys.2018.03.055
11. J. Aguado, D.P. Serano, J.M. Escola and A. Patel, *Anal. Appl. Pyrol.*, **85**, 352 (2009); https://doi.org/10.1016/j.jaap.2008.10.009
12. F.J. Passamonti and U. Sedran, *Appl. Catal. B, Environ.*, **125**, 499 (2012); https://doi.org/10.1016/j.apcatb.2012.06.020
13. M. Pérez, H. Armendáriz, J.A. Toledo, A. Vázquez, J. Navarrette, A. Montoya and A. Gárcia, *J. Mol. Catal. A: Chem.*, **149**, 169 (1999); https://doi.org/10.1016/S1381-1169(99)00172-7
14. Y. Kuwahara, W. Kaburagi, K. Nemoto and T. Fujitami, *Appl. Catal. A, Gen.*, **476**, 186 (2014); https://doi.org/10.1016/j.apcata.2014.02.032
15. A.K. Shah, M. Kumar, S.H.R. Abdi, R.I. Kureshy, N.H. Khan and H.C. Bajaj, *Appl. Catal. A, Gen.*, **486**, 105 (2014); https://doi.org/10.1016/j.apcata.2014.08.024
16. T. Barzetti, E. Selli, D. Moscotti and L. Forni, *J. Chem. Soc., Faraday Trans.*, **92**, 1409 (1996); https://doi.org/10.1039/ft9969201401
17. M. Ejtemaei, A. Tavakoli, N. Charchi, B. Bayati, A.A. Babaluo and Y. Bayat, *Adv. Powder Technol.*, **25**, 840 (2014); https://doi.org/10.1016/j.apt.2013.12.009
18. J.R. Sohn, J.G. Kim, T.D. Kwon and E.H. Park, *Langmuir*, **18**, 1666 (2002); https://doi.org/10.1021/la011304h
19. E. Djurado, P. Bouvier and G. Lucazeau, *J. Solid State Chem.*, **149**, 399 (2000); https://doi.org/10.1006/jssc.1999.8565
20. S.K. Das and S.A. El-Safty, *Chem. Cat. Chem.*, **5**, 3050 (2013); https://doi.org/10.1002/cctc.201300192
21. K.S. Sing, D.H. Everett, R.A.W. Haul, L. Moscou, R.A. Pierotti, J. Rouquérol and T. Siemieniewska, *Pure Appl. Chem.*, **57**, 603 (1985); https://doi.org/10.1351/pac198557040603
22. M. Thommes, K. Kaneko, A.V. Neimark, J.P. Oliver, F. Rodriguez-Reinoso, J. Rouquérol and K.S.W. Sing, *Pure Appl. Chem.*, **87**, 1051 (2015); https://doi.org/10.1515/pac-2014-1117
23. A. Suseno, K. Wijaya, W. Trisunaryanti and Roto, *Orient. J. Chem.*, **34**, 1427 (2018); https://doi.org/10.13005/ojc/340332